Spectroscopic Characterization of Intermediates in the Urate Oxidase Reaction[†]

Kalju Kahn and Peter A. Tipton*

Department of Biochemistry, University of Missouri-Columbia, Columbia, Missouri 65211

Received February 24, 1998; Revised Manuscript Received May 1, 1998

ABSTRACT: The oxidation of urate catalyzed by soybean urate oxidase was studied under single-turnover conditions using stopped-flow absorbance and fluorescence spectrophotometry. Two discrete enzyme-bound intermediates were observed; the first intermediate to form had an absorbance maximum at 295 nm and was assigned to a urate dianion species; the second intermediate had an absorbance maximum at 298 nm and is believed to be urate hydroperoxide. These data are consistent with a catalytic mechanism that involves formation of urate hydroperoxide from O_2 and the urate dianion, collapse of the peroxide to form dehydrourate, and hydration of dehydrourate to form the observed product, 5-hydroxyisourate. The rate of formation of the first intermediate was too fast to measure accurately at 20 °C; the second intermediate formed with a rate constant of 32 s^{-1} and decayed with a rate constant of 6.6 s^{-1}. The product of the reaction, 5-hydroxyisourate, is fluorescent, and its release from the active site occurred with a rate constant of 31 s^{-1}.

Urate oxidase (EC 1.7.3.3) is an enzyme involved in purine degradation which catalyzes the oxidation of urate to 5-hydroxyisourate with concomitant reduction of molecular oxygen to hydrogen peroxide. In tropical leguminous plants, such as soybean (*Glycine max*), the urate oxidase reaction is a part of the ureide pathway by which ammonia resulting from the action of nitrogenase is eventually converted to the ureides, allantoin and allantoate. The ureides serve as the vehicles for the transport of nitrogen thoughout the plant (*1*). In most mammals, the urate oxidase reaction is part of the pathway by which removal of excess nitrogen is facilitated by the conversion of relatively insoluble purines to allantoin. Interestingly, urate oxidase is absent in humans and other higher primates as a result of two mutations in the coding sequence which cause premature termination of translation (*2*). As a result, in higher primates uric acid is the end product of purine metabolism, and the level of uric acid or urate in human blood serum is substantial, usually several hundred micromolar (*3*). Elevated levels of urate have been associated with both positive and negative effects on human health. It has been shown that uric acid is an effective antioxidant and radical scavenger, both in vitro (*4*) and in vivo (*5*). On the basis of its antioxidant properties, it has been proposed that the lack of urate oxidase is evolutionarily advantageous, contributing to a longer life expectancy and decreased cancer rates (*6*). However, high urate levels in blood can cause gouty arthritis and renal stones (*7, 8*). Urate oxidase from *Aspergillus flavus* has successfully been used as a drug to treat hyperuricemic disorders (*9*).

The chemical mechanism of the urate oxidase reaction has not been established, and is particularly interesting in light of the fact that the enzyme neither contains nor requires any cofactor. Although urate oxidase has often been classified as a copper-dependent enzyme, it has been demonstrated that catalytically active enzyme from bacteria (*10*), yeast (*11*), fungi (*12*), and bovine liver (*13*) is free of copper. We have recently shown that urate oxidase from soybean root nodules does not contain copper or any other redox active metal; furthermore, the molecular mass was determined by MALDI-TOF[1] mass spectrometry and shown to match the mass predicted on the basis of the deduced amino acid sequence, indicating that no prosthetic group was present in the enzyme (*14*). The recently determined crystal structure of *A. flavus* urate oxidase complexed with azaxanthine confirms the absence of any cofactor in the active site (*15*).

The structural similarity between urate and reduced flavin suggests that the reaction of urate with molecular oxygen may proceed through intermediates similar to those encountered in flavin-dependent monooxygenases (*16*) (Scheme 1). In this mechanism urate and oxygen interact directly to form 5-hydroperoxyisourate as a discrete intermediate in the catalytic cycle. The putative 5-hydroperoxyisourate eliminates hydrogen peroxide to form dehydrourate, an analogue of oxidized flavin. Dehydrourate is then hydrated in the enzyme active site to form the observed product 5-hydroxyisourate, a structural analogue of 4a-hydroxyflavin. A number of experimental observations are consistent with the proposed mechanism. Isotopic tracer studies demonstrate that both atoms of oxygen in hydrogen peroxide originate from O_2 (*17*), and that the oxygen attached to C5 in 5-hydroxyisourate comes from water (*16*). The optical activity of 5-hydroxyisourate formed during the catalytic reaction indicates that water attacks an enzyme-bound intermediate.

[†] Supported by USDA Grant 96-35305-3542.

* Author to whom correspondence should be addressed. Telephone: (573) 882-7968. Fax: (573) 884-4812. E-mail: bctipton@muccmail.missouri.edu.

[1] Abbreviations: DTT, dithiothreitol; HIU, 5-hydroxyisourate; INT I, the first observed intermediate in the urate oxidase reaction; INT II, the second observed intermediate in the urate oxidase reaction; MALDI-TOF, matrix-assisted laser desorption ionization time-of-flight; OHCU, 2-oxo-4-hydroxy-4-carboxy-5-ureidoimidazoline; SVD, singular value decomposition; Tris, tris(hydroxymethyl)aminomethane.

S0006-2960(98)00446-2 CCC: $15.00
Published on Web 07/29/1998

Scheme 1

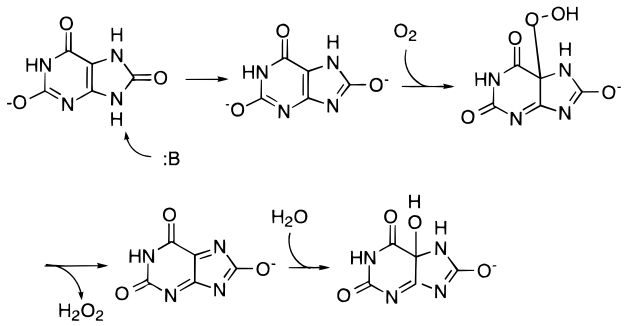

We report here the results of stopped-flow spectroscopic studies of the soybean urate oxidase reaction conducted under single-turnover conditions. The reaction was monitored by absorbance and by fluorescence; two discrete intermediates could be detected during the catalytic reaction, and their UV absorbance spectra were determined. The spectrum of one of these intermediates closely matches that expected for urate hydroperoxide.

MATERIALS AND METHODS

Purification of Urate Oxidase. Recombinant soybean urate oxidase (*14*) and a thioredoxin urate oxidase fusion protein (*16*) were expressed in *Escherichia coli* and purified as described previously, with the following modifications. The yield of soluble urate oxidase was increased by washing the cell paste after lysis twice with 100 mM Tris-Cl^-, pH 8.3, and additions of DTT and Triton X-100 to the buffer were omitted. Active fractions from the xanthine-agarose column were concentrated by ultrafiltration and degassed, and urate oxidase was precipitated by addition of ammonium sulfate to 65% saturation. The precipitate was pelleted by centrifugation at 20000*g* for 20 min, resuspended in the supernatant, and pelleted again under the same conditions. The pellet was redissolved in a minimal volume of 50 mM Tris-Cl^-, pH 8.2, and dialyzed extensively until no absorbance due to xanthine could be observed in the outer buffer. Protein concentration was determined by amino acid analysis at the University of Missouri Agricultural Experiment Station. An extinction coefficient of 62 000 M^{-1} cm^{-1} at 280 nm was determined for recombinant urate oxidase at pH 9.0, and this value was used in routine calculations of the enzyme concentration. Activity determinations during purification were carried out using a spectrophotometric assay in which urate consumption was monitored at 292 nm (*14*). The spectrophotometric assay underestimates the true rate of substrate disappearance since 5-hydroxyisourate also absorbs at this wavelength. The spectrophotometric rates were calibrated against the rates observed by monitoring the catalytic reaction with an oxygen electrode, and the true specific activity of the recombinant urate oxidase was found to be 6.1 μmol min^{-1} mg^{-1}. The specific activity of the thioredoxin fusion protein was 7.3 μmol min^{-1} mg^{-1}.

Analytical Ultracentrifugation of Urate Oxidase. Equilibrium ultracentrifugation studies of samples of urate oxidase at subunit concentrations of 3.9, 7.8, and 11.6 μM were conducted using an Optima XL-I analytical ultracentrifuge equipped with an An-50 Ti rotor. Samples were prepared in 50 mM Tris-SO_4^{2-} at pH 8.2. Equilibrium was achieved after 18 h by spinning at 10 000 rpm at 20 °C. Absorbance versus radius data were used to calculate the molecular mass of the holoenzyme using a value of 0.73 mL/g for the partial specific volume of urate oxidase (*18*).

Spectral Characterization of 5-Hydroxyisourate and Its Decomposition Product. The UV absorbance spectra of 5-hydroxyisourate (HIU) and the product of its hydrolysis, 2-oxo-4-hydroxy-4-carboxy-5-ureidoimidazoline (OHCU), were determined at pH 7.85 by converting 37 μM urate to 5-hydroxyisourate at 25 °C in the presence of 4 μM urate oxidase. Under these conditions, turnover of urate was complete in several seconds. The decomposition of 5-hydroxyisourate was monitored for 12 min with a Hewlett-Packard 8452A spectrophotometer over the spectral range of 240 to 330 nm. The data set which consisted of absorbance values at 2 nm intervals as a function of time was analyzed in a stepwise manner as follows. The initial estimate of the rate constant for the hydrolysis of 5-hydroxyisourate was obtained by fitting data from 304 to 330 nm to a single-exponential model. The observed absorbance in this region follows first-order kinetics due to the fact that OHCU does not absorb above 300 nm. Since OHCU does absorb below 300 nm, data obtained between 240 and 300 nm were fitted to a model which accounted for that absorbance; that is, the data were fitted to the analytical expression describing the sequential process HIU → OHCU → decomposition product. The absorbance of the solution at any point in time is given by Lambert−Beer's law (eq 1) where A is the absorbance divided by the path length, ϵ_{HIU}, ϵ_{OHCU}, and ϵ_{decomp} are the extinction coefficients for 5-hydroxyisourate, OHCU, and the decomposition product, respectively, and C_{HIU}, C_{OHCU}, and C_{decomp} are their concentrations.

$$A = \epsilon_{HIU}C_{HIU} + \epsilon_{OHCU}C_{OHCU} + \epsilon_{decomp}C_{decomp} \quad (1)$$

The analytical expressions for the concentrations of each species as a function of time in unimolecular sequential reactions are known and can be substituted into eq 1 (*19*); upon rearrangement eq 2 is obtained.

$$\frac{A}{[HIU]_0} = Coeff_1 e^{-k_1 t} + Coeff_2 e^{-k_2 t} + Coeff_3 \quad (2)$$

The coefficients in this expression are defined by eqs 3−5.

$$Coeff_1 = \epsilon_{HIU} - \frac{\epsilon_{OHCU}k_1 - \epsilon_{decomp}k_2}{k_1 - k_2} \quad (3)$$

$$Coeff_2 = \frac{k_1}{k_1 - k_2}(\epsilon_{OHCU} - \epsilon_{decomp}) \quad (4)$$

$$Coeff_3 = \epsilon_{decomp} \quad (5)$$

Experimental data at discrete wavelengths were fitted to eq 2 in which the value of k_1 was fixed at the value determined by analysis of the data obtained above 304 nm. The fitting was accomplished using the program IGOR Pro (WaveMetrics, Inc.). The sum of the three coefficients of eq 2 are equal to ϵ_{HIU}, so evaluation of eq 2 at discrete wavelengths allows the reconstruction of the absorbance spectrum of 5-hydroxyisourate.

The values for the extinction coefficients of HIU obtained from this analysis were used as initial estimates in the global numerical fitting of the complete wavelength data set,[2] which was accomplished using the program DYNAFIT (*20*). The input consisted of a set of chemical equations describing the sequential process HIU → OHCU → decomposition product, initial concentrations of each species, initial estimates of the rate constants, initial estimates of extinction coefficients, and the experimental data obtained between 20 and 720 s. An abbreviated data set which consisted of the experimental data collected between 20 and 200 s was analyzed in terms of a simpler model which assumed that decomposition of OHCU was negligible in this time interval. Thus, the abbreviated multiwavelength data set was fitted to the single-step process HIU → OHCU using DYNAFIT.

The kinetics of decomposition of optically active 5-hydroxyisourate was also studied by monitoring the reaction by circular dichroism. A solution of 541 μM urate was converted to 5-hydroxyisourate by the action of urate oxidase at pH 7.6, 25 °C, and the CD data were recorded using an AVIV 62DS CD spectropolarimeter. The CD signals at 306 and 260 nm were fitted to the single-step model and to the two-step model (eq 2), respectively.

The fluorescence spectrum of enzymatically generated 5-hydroxyisourate was recorded using a Aminco SLM 8100 spectrofluorimeter with excitation at 306 nm. Suitable buffer blanks were subtracted from experimental data in all spectroscopic investigations.

Stopped-Flow Kinetics Data Collection. Pre-steady-state kinetic studies were performed using a KinTek SF-2000 spectrophotometer/spectrofluorimeter equipped with a 2.6 cm path length observation cell, a photodiode for single-wavelength absorbance detection, and a photomultiplier tube for fluorescence detection. The instrument dead-time was determined to be 4 ms (*21*). For each reaction 400 data points were collected within 500 ms, followed by an additional 100 data points up to 2 s; 6−10 traces were averaged to obtain time courses that were used for fitting. Blank spectra were collected by mixing urate with reaction buffer or by mixing enzyme with reaction buffer; the absorbance of the blank spectra was time-independent after 10−15 ms. Single-turnover reactions were conducted by mixing together 9.35 μM urate in 50 mM Tris-SO_4^{2-} containing 100 μM Cl^-, pH 7.0, with 22 μM urate oxidase in 50 mM Tris containing 100 μM Cl^-, pH 8.75. The pH of the resulting solution was 7.85, which was selected as the optimal pH to satisfy the contrary constraints of 5-hydroxyisourate, which decomposes faster at higher pH values, and urate oxidase, which is decreasingly soluble at lower pH values. The time course of the reaction was monitored by absorbance measurements between 290 and 425 nm at 20 °C. The fluorescence emission was monitored simultaneously using a 25 nm bandwidth filter centered at 400 nm. The urate oxidase−thioredoxin fusion protein, which is more soluble than unmodified urate oxidase, was used in experiments in which the urate concentration was varied. Urate concentrations after mixing were 5, 9.5, 15, and 19 μM; the enzyme concentration after mixing was 30 μM. The reactions were conducted at 16.5 °C in 100 mM Tris-Cl^-, pH 8.4, and the absorbance at 304 nm was monitored. The effect of urate concentration was also investigated with 6 μM recombinant urate oxidase at 314 nm (absorbance and fluorescence emission using exitation at 314 nm). These reactions were performed at 25 °C in 100 mM Tris-Cl^-, pH 8.0; the urate-to-enzyme ratio was varied from 0.39 to 13.1.

Stopped-Flow Kinetics Data Analysis. The UV absorbance spectra of the intermediates in the catalytic cycle and the rate constants for their interconversion were obtained by a multistep procedure in which the time traces collected at 18 discrete wavelengths between 290 and 330 nm were combined into a single data set, represented by the matrix **A**. The number of observable species occurring during the reaction and the initial estimates of their extinction coefficients were obtained by singular value decomposition analysis using the program IGOR Pro (Wavemetrics, Inc.). Treatment of the multivariate data set **A** by SVD analysis (*22, 23*) decomposes the data into a family of pairs of basis spectra and amplitude vectors, as well as a quantitative measure of the significance of each pair. The number of discrete species contributing to the absorbance of the sample during the catalytic reaction was determined by visual inspection of the signal-to-noise in the basis spectra and amplitude vectors, consideration of the magnitude of the significance parameters, and by determining the minimum number of pairs of basis spectra and amplitude vectors that were required to satisfactorily reconstruct the observed data. The initial estimates of the rate constants governing the interconversion of the species were obtained by nonlinear least-squares fitting of the amplitude vectors to the function describing three first-order reactions (eq 6).

$$Y_{tot} = Y_1 e^{-k_1 t} + Y_2 e^{-k_2 t} + Y_3 e^{-k_3 t} + C \qquad (6)$$

In eq 6, Y_{tot} is the magnitude of the amplitude vector, and C is a constant. Y_1, Y_2, and Y_3 are complex functions which are not related to physical parameters such as extinction coefficients and rate constants in any simple manner. The rate constants derived from this analysis and the initial concentration of urate were used to construct a matrix **C** that contained the concentrations of each species as a function of time. The extinction coefficients were obtained by solving the generalized form of Lambert−Beer's Law, $\mathbf{A} = \mathbf{E} \bullet \mathbf{C}$, using the original data matrix **A** and the derived concentration matrix **C** (*24*). The final absorbance spectra of the enzymatic intermediates and the final values for the rate constants were obtained by performing a global fit (*25*) of the multiwavelength data between 290 and 330 nm to the three-step model INT I → INT II → HIU → OHCU using the program DYNAFIT (*20*). The rate constants and extinction coefficients for INT I and INT II were optimized simultaneously; the extinction coefficients for HIU and OHCU were fixed to values determined independently. The goodness of fit was judged by the distribution of residuals (visual inspection of residuals plots and Kolmogorov−Smirnov statistics) and by the value of reduced χ^2 (defined in DYNAFIT as the weighted sum of squared deviations divided by the number of points; a good fit gives χ^2 close to unity) (*26*). The adequacy of the three-step model was evaluated by comparing the final χ^2 from this model with χ^2 from a two-step

[2] DYNAFIT limits the number of progress curves that can be fitted simultaneously to 16; therefore, the global data set consisting of 45 time courses obtained at 2 nm intervals was divided into subsets which were fitted.

INT I → INT II → HIU) and a four-step (INT I → INT II → HIU → X → OHCU) model using the F-test (*27*). The independence of the rate constants was checked by analyzing the correlation matrix and the matrix of redundancy grades (*20*).

The fluorescence time traces were fitted to the four-step model INT I → INT II → HIU → HIU* → OHCU using DYNAFIT. In this model HIU is enzyme-bound 5-hydroxyisourate and HIU* is free 5-hydroxyisourate, so the step HIU → HIU* represents product dissociation. During the fitting of the data to this model, only the rate constant for dissociation and the fluorescence response coefficient for HIU* were varied, while the fluorescence response coefficients for the other species were set to zero and the other rate constants were fixed to the values obtained from global fitting of the absorbance data.

RESULTS

Quaternary Structure of Urate Oxidase. The molecular mass of recombinant soybean urate oxidase was examined by equilibrium ultracentrifugation. Samples at subunit concentrations of 3.9, 7.8, and 11.6 μM yielded molecular mass estimates of 136 300 ± 1100 Da, 137 700 ± 900 Da, and 141 600 ± 1200 Da, respectively. The subunit molecular mass of urate oxidase calculated from the deduced amino acid sequence is 35 052 Da, suggesting that the enzyme is tetrameric under the conditions of the stopped-flow kinetics experiments. The molecular mass of soybean urate oxidase holoenzyme has earlier been estimated to be 68 000 Da (*28*) and 105 000 Da (*29*) based on gel filtration chromatography, and 124 000 Da based on analytical ultracentrifugation measurements (*30*). The crystal structure of the *Aspergillus niger* urate oxidase revealed that it is a tetramer, with one inhibitor molecule bound to each subunit (*15*). The discrepancy between previous analytical ultracentrifugation results and those presented here is probably related to the underestimation of the value of the partial specific volume of the enzyme (*30*); the low values obtained by gel filtration chromatography may have been caused by partial dissociation of the holoenzyme.

Absorbance and Fluorescence Spectra of 5-Hydroxyisourate. An accurate determination of the absorbance spectrum of 5-hydroxyisourate is complicated by the fact that it overlaps with the spectrum of urate and its decomposition products (Figure 1). However, a clean spectrum of 5-hydroxyisourate can be obtained by rapidly oxidizing urate enzymatically using a high concentration of urate oxidase and correcting the observed spectrum for the contributions from decomposition products. The extinction coefficient of the other product of the enzymatic reaction, hydrogen peroxide, is 2 orders of magnitude smaller than that of 5-hydroxyisourate and can be neglected (*31*). 5-Hydroxyisourate is unstable and undergoes hydrolysis to form OHCU in neutral aqueous solutions; OHCU is also unstable and decomposes eventually to form allantoin (*16*). The decomposition of 5-hydroxyisourate follows first-order kinetics when the process is monitored spectrophotometrically at 304−330 nm where 5-hydroxyisourate is the only absorbing species, and the rate constant for its hydrolysis was estimated to be 2.1×10^{-3} s^{-1}. The same value was obtained from the analysis of the CD signal at 306 nm. The analytical

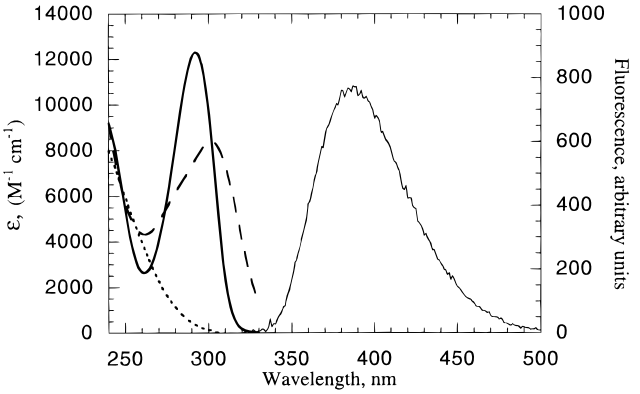

FIGURE 1: The experimentally determined UV absorbance spectrum of urate (thick solid line), the calculated spectra of 5-hydroxyisourate (dashed line), and decomposition products of 5-hydroxyisourate at short times (dotted line) at pH 7.85 and the experimentally determined fluorescence emission spectrum of 5-hydroxyisourate (thin solid line) at pH 7.5 with excitation at 306 nm. The calculated UV spectrum of 5-hydroxyisourate is corrected for contributions from decomposition products; the calculated UV spectrum of the decomposition products is dominated by absorbance due to 2-oxo-4-hydroxy-4-carbohydroxy-5-ureidoimidazoline.

fitting of absorbance versus time data from 240 to 330 nm to eq 2 yielded the spectrum of 5-hydroxyisourate with λ_{max} at 302 nm and an estimate of the first-order rate constant for the decomposition of OHCU of 2.2×10^{-3} s^{-1}. The value of this rate constant was poorly determined, however, and a more accurate estimate of k_2, $1.2 \pm 0.1 \times 10^{-3}$ s^{-1} was obtained from the analysis of the CD signal at 260 nm. The spectrum of OHCU cannot be accurately estimated from eq 2 since the two rate constants describing its formation and decomposition are similar; numerical fitting of the experimental data to the two-step model did not give satisfactory convergence either. We thus obtained the approximate spectrum of OHCU that was not corrected for contributions from decomposition products by global fitting of the first 200 s of absorbance data to the single step HIU → OHCU model. This approximation is adequate for the analysis of urate oxidase reaction kinetics since decomposition of OHCU is negligible on the time scale of the stopped-flow experiments. The spectrum of 5-hydroxyisourate that was obtained by global numerical fitting to the single-step model was very similar to the spectrum obtained by analytical fitting of individual absorbance traces to eq 2. The difference between the calculated spectrum of 5-hydroxyisourate and the first observed spectrum at 20 s was no more than 5% at any wavelength. The approximate absorbance spectrum of the urate oxidase reaction product has been reported before (*32*) and is similar to that of 5-hydroxyisourate reported here.

Time Course of the Urate Oxidase Reaction. The formation and decay of 5-hydroxyisourate was monitored at 304 and 314 nm as a function of urate concentration in the presence of excess urate oxidase. The apparent rate constant for 5-hydroxyisourate formation and the time required for the maximal absorbance to be reached were independent of the concentration of urate indicating that association of urate oxidase and urate was complete within the mixing time of the experiment, and that the reaction was proceeding under true first-order conditions, i.e., all of the substrate was bound to the enzyme. When urate concentrations were close to or exceeded the molar concentration of enzyme active sites, the

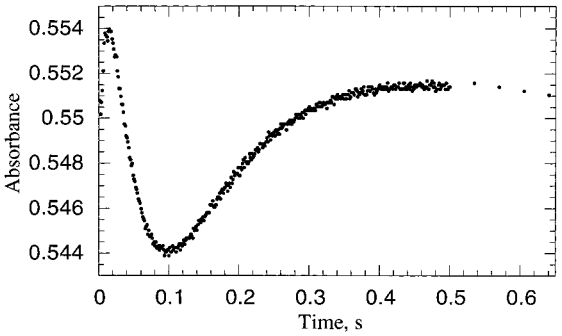

FIGURE 2: Stopped-flow absorbance time trace at 306 nm for the reaction between 9 μM urate and 24 μM thioredoxin−urate oxidase at 15 °C, 100 mM Tris-Cl$^-$, pH 8.0.

absorbance and fluorescence maxima occurred later indicating the occurrence of multiple turnovers. It was found that enzyme-to-substrate ratios of 2−3 were optimal for spectral characterization of enzymatic intermediates.

When the absorbance of the reaction was monitored at 304−306 nm, four kinetically distinguishable phases could be observed (Figure 2). The first phase, characterized by an increase in absorbance, was of short duration and was clearly observed only at reduced temperature. The apparent first-order rate constant k_{obs} was estimated to be >64 s^{-1} for this phase at 7.8 °C. The second phase, characterized by a decrease in the absorbance occurred between 20 and 70−90 ms. Increasing the urate concentration from 5 to 19 μM in the presence of 30 μM enzyme active sites resulted in only a very small change in the position of the absorbance minimum and did not affect the observed first-order rate constant. These data suggest that the second phase describes the conversion of the first enzyme bound intermediate to the second intermediate. The observed first-order rate constant for this step was independent of pH but varied strongly with temperature, being 12 ± 2 s^{-1} at 7.8 °C and 38 ± 2 s^{-1} at 20 °C. The third phase, characterized by an increase in absorbance, lasted from 80 ms to 350−400 ms, and its duration was also independent of urate concentration. The apparent first-order rate constant was 7.2 ± 0.6 s^{-1} at 20 °C and did not show significant temperature dependence. This phase appears to correspond to the conversion of the second enzymatic intermediate to the product. The final phase, spontaneous decomposition of the enzymatic reaction product, is much slower than the enzymatic steps; the first-order rate constant was found to be temperature and pH dependent in accord with previously published observations (*32*).

Spectral Characterization of the Enzyme-Bound Intermediates. The absorbance spectra of enzyme-bound intermediates were extracted from absorbance versus time data sets collected between 290 and 330 nm, as described above. The reactions were conducted under single-turnover conditions in which each step in the observed reaction sequence is a first-order process.

SVD analysis indicated that the absorbance of the sample arose from four components, and the absorbance data from 19 to 1000 ms were well described by the three-step model INT I → INT II → HIU → OHCU. The data obtained during the first 19 ms were neglected in the analysis of these data sets, because the number of data points describing the initial rapid phase of the reaction was small, and blank traces (enzyme + buffer) showed a small increase in absorbance

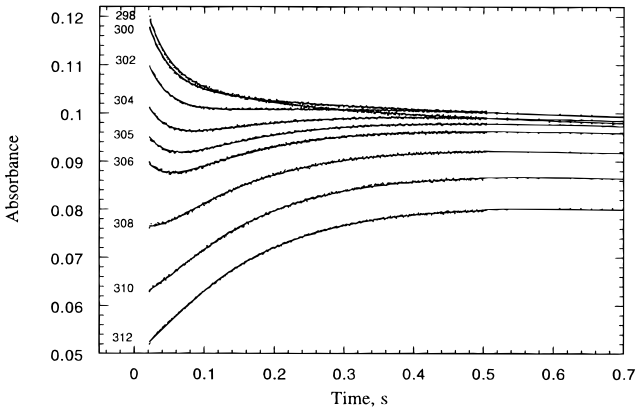

FIGURE 3: Observed and fitted absorbance time traces from 298 to 312 nm for the urate oxidase reaction conducted at 20 °C. After mixing, solutions contained 4.7 μM urate and 11 μM recombinant urate oxidase, 50 mM Tris-SO_4^{2-}, 100 μM Cl$^-$, pH 7.85. The sequential model INT I → INT II → HIU → OHCU was used for fitting the multiwavelength absorbance data, as described in the text.

(ca. 20% of that observed in the presence of substrate) during the first 10−15 ms. Neglecting the earliest time points also ensures that only first-order processes are represented in the data. Global fitting of the multiple wavelength data yielded values for the three rate constants for the model INT I → INT II → HIU → OHCU and their 1σ confidence intervals of 31.6 ± 0.7 s^{-1}, 6.60 ± 0.02 s^{-1}, and 0.0490 ± 0.0003 s^{-1} (Figure 3).[3] In our experience the variation in the values of the rate constants from experiment to experiment was greater than the confidence intervals obtained from the analysis of a single data set, and we estimate that errors in the rate constants on the order of 10% of their magnitude are more accurate. The value of χ^2 for this model was significantly smaller than for the two-step model where the hydrolysis of HIU to OHCU was omitted (0.90 versus 9.86, respectively). The residuals plots and Kolmogorov−Smirnov statistics also indicated that a good fit was achieved with the three-step model. No interdependencies of rate constants could be detected from the analysis of the correlation matrix. Fitting the global absorbance data set to a four-step model was hampered by poor convergence and interdependency of rate constants. When the data at a single wavelength, 304 nm, were fitted to the four-step model, an insignificant reduction in χ^2 (0.489) was observed, compared to when the data were fitted to a three-step model (χ^2, 0.495).

Some care is required in the assignment of the values determined for the rate constants to individual reaction steps. When all participating species in a sequential mechanism contribute to the absorbance, multiple solutions exist for the equation which describes the absorbance; the different solutions correspond to assigning the rate constants to different steps and result in different calculated spectra for each species (*19*). For example, six different spectra for B and three different spectra for C satisfy absorbance data for

[3] We do not know why the value of the rate constant for the decay of 5-hydroxyisourate determined in stopped-flow experiments is different from the value determined by standard spectrophotometric assays conducted over several minutes. However, we have observed that the decay of 5-hydroxyisourate is efficiently catalyzed by many compounds, and it is possible that our stopped-flow cell contained minute quantities of such a catalyst.

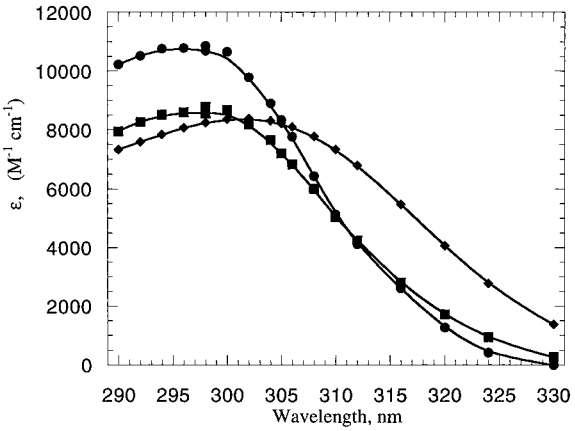

FIGURE 4: Absorbance spectra of the enzymatic intermediates INT I (●) and INT II (■), and the product 5-hydroxyisourate (◆) calculated from the time courses obtained between 290 and 330 nm.

the model A → B → C → D where A, B, and C contribute to the absorbance and the assignment of rate constants to reaction steps cannot be made a priori. In the present case, the analysis is significantly simplified since the slowest rate constant can be assigned with confidence to the last step, HIU → OHCU. For this situation, only two solutions exist; that is, the data can be fitted equally well if the process INT I → INT II is assigned the fastest rate constant (32 s^{-1}) and the process INT II → HIU is assigned the other rate constant (6.6 s^{-1}), or if the two rate constants are interchanged. Interchanging the two rate constants leads to different calculated spectra for INT II, however, which allows one to make a reasonable choice between the possible assignments. It was found that the assignment of the faster step to INT I → INT II and the slower step to INT II → HIU produced a spectrum of INT II which did not vary under different experimental conditions. The reverse order of the two rate constants yielded a spectrum of INT II that varied with experimental conditions and which was characterized by $\epsilon_{max} \approx 4000\ M^{-1}\ cm^{-1}$, which is too low for a purine derivative. It should be noted, however, that the spectra of INT I and HIU, as well as the overall goodness of fit, as reflected in the value of χ^2, were identical in the two situations described above. The final calculated spectra of the two enzymatic intermediates, INT I and INT II, and the reaction product, HIU, are shown in Figure 4. The high absorbance due to urate oxidase prevented extending the data below 290 nm. No transient species were observable above 330 nm in single-turnover experiments. Spectral and kinetic properties of the compounds characterized by the stopped-flow experiments are summarized in Table 1.

Urate Oxidase Turnover Detected by Fluorescence. The product of the urate oxidase reaction, 5-hydroxyisourate, is fluorescent when excited at 300−320 nm. The emission maximum is located at 380−400 nm (Figure 1). Urate has been reported to be fluorescent under a N_2 atmosphere (*33*), but we could not observe any fluorescence from uric acid or urate monoanion in air-saturated aqueous solutions. When the concentration of urate was varied in the presence of excess urate oxidase, the fluorescence maximum attained during the course of the reaction was proportional to the initial urate concentration (data not shown). The observation that 5-hydroxyisourate is fluorescent provides a convenient method to monitor the catalytic reaction without interference from substrates or enzyme-bound intermediates. As shown in Figure 5, the fluorescence signals arising from excitation between 302 and 330 nm displayed a distinct lag. The duration of the lag phase suggested that only free 5-hydroxyisourate contributed to the fluorescence signal. The fluorescence traces between 22 and 1000 ms were fitted as a single composite data set to the extended model INT I → INT II → HIU → HIU* → OHCU where only HIU* is fluorescent. The F-test indicated that for the analysis of the fluorescence data, the extended model (χ^2, 0.321) was significantly better than the model that does not include product dissociation (χ^2, 2.37). From this analysis a value of 31.3 ± 0.7 s^{-1} for the rate constant for HIU → HIU*, i.e., product dissociation, was obtained. The fact that the fluorescence signals obtained at different excitation wavelengths could be fitted by a single model supports the conclusion that only one fluorescent species was present in the reaction solutions.

Table 1: Characteristics of Proposed Intermediates and Products of the Urate Oxidase Reaction

species	structure	λ_{max} (nm)	formation rate constant (s^{-1})
INT I	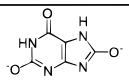	295-297	> 64
INT II	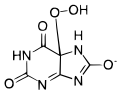	298	32
HIU	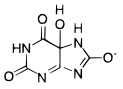	302	6.6
OHCU	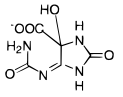	< 240	$2.1 \cdot 10^{-3}$

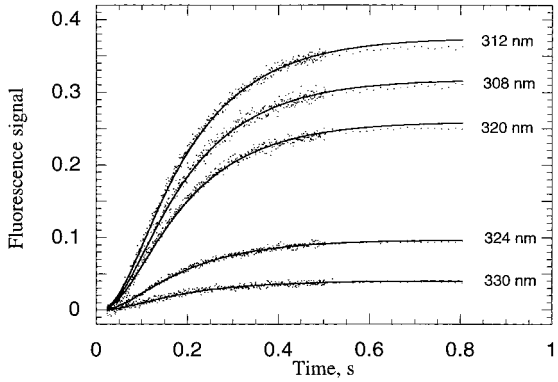

FIGURE 5: Observed and fitted fluorescence time traces for the urate oxidase reaction conducted at 20 °C. After mixing, each solution contained 4.7 μM urate and 11 μM recombinant urate oxidase, 50 mM Tris-SO_4^{2-}, 100 μM Cl^-, pH 7.85. The excitation wavelengths are indicated in the figure; the data were fitted as described in the text.

DISCUSSION

The chemical mechanism of the enzymatic oxidation of urate has not been defined previously but is of considerable interest given the unusual lack of redox cofactors in urate oxidase. Previous steady-state kinetic studies (*12*, *14*, *34*) have shown that a ternary urate−enzyme−oxygen complex

forms, and a sequential binding model with urate adding to the enzyme first has been proposed for soybean urate oxidase (*14*).

The structural similarity between urate and reduced flavin makes a mechanism for oxidation of urate that is analogous to flavin oxidation an attractive possibility. The reduction of O_2 by flavin proceeds via sequential single-electron transfers (*35*); the ability of flavin to stabilize an unpaired electron is responsible for its facile reaction with O_2. Transfer of the first electron from flavin to O_2 generates a caged radical pair which collapses to form the flavin hydroperoxide. Urate is also able to form a relatively stable radical anion, which has been generated enzymatically by horseradish peroxidase and observed at physiological pH by EPR (*36*). Scheme 1 illustrates how the flavin (or pterin) chemistry analogy can be applied to the urate oxidase reaction. One of the key features of the mechanism is that a urate hydroperoxide intermediate is postulated. Decomposition of the hydroperoxide would yield dehydrourate, which would lead to the observed product, 5-hydroxyisourate, upon hydration.

The crystal structure of *Aspergillus flavus* urate oxidase[4] was recently determined, and an alternative mechanism for the catalytic reaction was proposed in which it was suggested that urate oxidation proceeds via direct electron transfer from urate to O_2, either in concert with attack of water at C5 of urate, or prior to attack by water (*15*). This mechanism is consistent with isotopic tracer data, but differs significantly from the mechanism proposed above in that it posits no covalent adducts between urate and O_2.

Stopped-flow spectroscopy offers the opportunity to examine the nature of intermediates formed during turnover of urate oxidase. However, interpretation of stopped-flow absorbance data can be influenced strongly by the model to which the data are fitted. Therefore, care was taken to examine alternative models and to explore different data fitting techniques. In this regard, a heuristic approach such as that offered by SVD analysis is particularly useful, because it does not require a priori assumption of a kinetic model in the way required by global data fitting using computer programs such as DYNAFIT (*20*), or FITSIM (*38*). SVD analysis indicated that the absorbance of the reaction solution during the time scale of the stopped-flow experiment arose from four species. This conclusion was derived from visual inspection of the signal-to-noise of the basis spectra derived from the SVD analysis and the magnitude of their significance parameters, and from the finding that reconstruction of the experimental data required a minimum of four basis spectra with their associated amplitude vectors.

Analysis of the spectra of the four species detected during the single-turnover experiments, as well as consideration of the time dependence of their formation and decay, led to the conclusion that the absorbance arises from two enzyme-bound intermediates, the reaction product 5-hydroxyisourate, and 2-oxo-4-hydroxy-4-carboxy-5-ureidoimidazoline, which arises from nonenzymatic hydrolysis of 5-hydroxyisourate. The substrate urate is not detected in the experiments described here, and has presumably reacted within the mixing-time of the instrument. The first intermediate, whose formation can be seen clearly at reduced temperature (Figure 3), is characterized by an absorption maximum at 295−297 nm with $\epsilon_{max} \approx 11{,}000\ M^{-1}\ cm^{-1}$ (Figure 4). We propose that this intermediate, which corresponds to INT I in the model to which the data were fitted, is a urate dianion bound to the enzyme. The UV spectrum of INT I is more similar to the spectrum of the urate dianion ($\lambda_{max} = 295$ nm) than to urate monoanion ($\lambda_{max} = 292$ nm) in aqueous solution (*39*). The chromophore in urate is the [$N_3^--C_4{=}C_5-C_6{=}O_6 \leftrightarrow N_3{=}C_4-C_5{=}C_6-O_6^-$] moiety (*40*), and model studies suggest that the environment around urate may influence its UV spectrum. The study of solvent effects on the spectrum of uric acid ($\lambda_{max} = 280$ nm in trifluoroacetic acid, 284 nm in water, 290 nm in DMSO, 294 nm in hexamethylphosphoramide) demonstrates that the position of the low-energy spectral maximum is red-shifted when uric acid donates a hydrogen bond to the solvent; a small blue-shift may occur when uric acid accepts a hydrogen bond. The crystal structure of *A. flavus* urate oxidase suggests that the C6 carbonyl of urate accepts a hydrogen bond from Arg176, so the spectral data are more consistent with the notion that INT I is a urate dianion than a red-shifted urate monoanion.

It has been suggested previously that a urate dianion forms during the catalytic cycle (*14*). In nonenzymatic solution studies the urate dianion undergoes oxidation much more rapidly than the monoanion (*41*), and the rate of spontaneous oxidation is dependent on the oxygen concentration. A ^{13}C NMR titration study (*16*) and UV spectrophotometric comparisons of different urate derivatives (*39*) indicate that in alkaline aqueous solution the N3,N9-deprotonated urate dianion predominates. The N3-deprotonated monoanion is the predominant form in aqueous solution at pH 6−10, and steady-state kinetic studies have established that urate oxidase binds the urate monoanion as the true substrate. The pH dependence of the kinetic parameters has also provided evidence that the enzyme has a catalytic residue which abstracts a proton from the substrate, resulting in the formation of the urate dianion at the active site (*14*).

The second observable intermediate in the catalytic reaction, corresponding to INT II in the model to which the data were fitted, has an absorption maximum at 296−298 nm with an extinction coefficient of 8200−8600 $M^{-1}\ cm^{-1}$. Comparisons with the spectra of the urate neutral radical, urate anion radical, and urate dianion radical (*4*) clearly show that INT II is not a radical species. Based on the mechanisms that have been proposed for the urate oxidase reaction, structures for INT II that may be considered include 5-hydroperoxyisourate, by analogy with well-established flavin chemistry (*35, 42*), and tautomers or ions of dehydrouric acid, which would result from direct transfer of two electrons from urate to O_2 (Scheme 2).

Dehydrouric acid (*43*) can exist in two tautomeric forms, *para*-quinoid $\Delta^{3,4}$ -dehydrouric acid and *ortho*-quinoid $\Delta^{4,9}$ -dehydrouric acid; for the dehydrourate anion only one highly resonance-stabilized form is possible. The 1,3-dimethyl derivative of $\Delta^{4,9}$-dehydrouric acid has been synthesized and is characterized by absorbance maxima at 290 and 366 nm (*44*). The methylation of both N1 and N3 in purines is known to cause only a small shift to longer wavelengths in the position of the absorption maximum arising from the π

[4] Soybean urate oxidase and *Aspergillus flavus* urate oxidase share approximately 40% sequence identity, but motifs which are conserved throughout most of the 20 or so urate oxidases that have been sequenced are shared (*37*).

Scheme 2

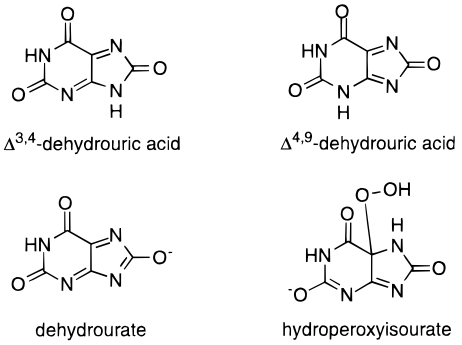

→ π^* transition (*40*), and since INT II does not have any absorbance bands above 330 nm it is unlikely to be the *ortho*-quinoid tautomer of dehydrouric acid. The dehydrourate anion is not a likely candidate for INT II since, in the spectra of derivatives of uracil, uric acid, and analogous lumazines, deprotonation of the parent acid is accompanied by a bathochromic shift (*39*, *40*, *45*).

6,6-Dimethyldihydropterin (*46*), a stable analogue of dihydrobiopterin, exists in the *para*-quinoid tautomeric form (*47*) and can serve as a model for $\Delta^{3,4}$-dehydrouric acid. A comparison of the spectra of 5-hydroxy-9-methylisouric acid (*48*) (a hydrated analogue of $\Delta^{3,4}$-dehydrouric acid) and 4a-hydroxy-6-methylpterin (*49*) indicates that replacing an oxo group at the 2-position with an amino group causes a slight red-shift in the absorption maximum. Neutral 6,6-dimethyldihydropterin has an absorption maximum at 303 nm and a shoulder at 350 nm in aqueous solution. Therefore, $\Delta^{3,4}$-dehydrouric acid would be expected to have one UV absorbance peak between 290 and 300 nm and another peak or shoulder around 340−350 nm. INT II displayed only one peak with a maximum at 296−298 nm, and therefore does not appear to be assignable to either dehydrouric acid tautomer or to dehydrourate.

An authentic sample of 5-hydroperoxyisourate is not available for comparison with the spectrum of INT II. However, evidence that 5-hydroperoxyisourate is a plausible candidate for INT II can be adduced from comparisons of the spectroscopic properties of homologous compounds. The UV absorbance spectra of the 4a-hydroxy and 4a-hydroperoxy derivatives of 6-methyl-5-deazapterin differ only by 2 nm in their absorption maxima (*50*). Similarly, the absorbance maxima of 4a-hydroxy and 4a-hydroperoxy flavins differ by less than 10 nm (*51*−*53*). The absorbance maximum of 5-hydroxyisourate is 302 nm (Figure 1) and that of INT II is around 298 nm. Thus, all the available experimental evidence is consistent with INT II being assigned to 5-hydroperoxyisourate.

The observation of discrete intermediates during the urate oxidase reaction suggests that a concerted reaction in which water attack at C5 occurs simultaneously with direct electron transfer from urate to O_2 is not tenable (*15*). A stepwise version of this mechanism in which transfer of two electrons from urate generates $\Delta^{3,4}$-dehydrouric that is subsequently attacked by water and rapidly deprotonated seems unlikely. The simultaneous transfer of two electrons from singlet urate dianion to triplet dioxygen violates the spin-conservation rule (*54*). Reaction between urate and dioxygen via single-electron transfer would generate a radical pair whose collapse into 5-hydroperoxyisourate would be expected to be extremely rapid; it is not clear how the enzyme could force the reaction onto a pathway in which transfer of the second electron from the urate radical to superoxide would be favored over radical recombination.

We believe that the most likely mechanism for the urate oxidase reaction involves single-electron transfer from dianionic urate, which has a one-electron redox potential of 0.26 ± 0.02 V(*55*), to oxygen to form a urate radical anion and superoxide. Radical recombination would lead to formation of 5-hydroperoxyisourate. Elimination of hydrogen peroxide from 5-hydroperoxyisourate would yield dehydrourate, which was not observed experimentally. Dehydrourate has been generated in aqueous solutions electrochemically, and shown to undergo hydration to form 5-hydroxyisourate with a rate constant of 32.5 s^{-1} (*56*). Therefore, even if urate oxidase does not accelerate the rate of this step, dehydrourate would not be expected to accumulate to detectable levels during turnover.

The lag in the fluorescence time courses (Figure 5) suggests that enzyme-bound 5-hydroxyisourate does not fluoresce as strongly as the species free in solution. The crystal structure of urate oxidase shows that the inhibitor 8-azaxanthine lies above Phe159 (*15*), which could provide an efficient means to quench the fluorescence of 5-hydroxyisourate at the active site.

ACKNOWLEDGMENT

We are grateful to Professor Michael Henzl for assistance with the ultracentrifugation experiments.

REFERENCES

1. Reynolds, P. H. S., Boland, M. J., Blevins, D. G., Randall, D. D., and Schubert, K. R. (1982) *Trends Biochem. Sci. 7*, 366−368.
2. Wu, X. W., Muzny, D. M., Lee, C. C., and Caskey, C. T. (1992) *J. Mol. Evol. 34*, 78−84.
3. Becker, B. F. (1993) *Free Rad. Biol. Med. 14*, 615−631.
4. Simic, M. G., and Jovanovic, S. L. (1989) *J. Am. Chem. Soc. 111*, 5778−5782.
5. Frei, B., England, L., and Ames, B. N. (1989) *Proc. Natl. Acad. Sci. U.S.A. 86*, 6377−6381.
6. Ames, B. N., Cathcart, R., Schwiers, E., and Hochstein, P. (1981) *Proc. Natl. Acad. Sci. U.S.A. 78*, 6858−6862.
7. Smyth, C. J. (1975) *Arthritis Rheum. 18*, 713−719.
8. Terkeltaub, R. A. (1996) *Sc. Med. 3*, 22−31.
9. Rozenberg, S., Roche, B., Koeger, A. C., Borget, C., Wrona, N., and Bourgeois, P. (1995) *Rev Rhum, Eng. Ed. 62*, 392−394.
10. Bongaerts, G. P. A., Uitzetter, J., Brouns, R., and Vogels, G. D. (1978) *Biochim. Biophys. Acta 527*, 348−358.
11. Nishimura, H., Yoshida, K., Matsushima, A., and Inada, Y. (1982) *J. Biochem. 91*, 41−48.
12. Conley, Y. G., and Priest, D. G. (1980) *Biochem. J. 187*, 727−732.
13. Truscoe, R., and Williams, V. (1965) *Biochim. Biophys. Acta 105*, 292−300.
14. Kahn, K., and Tipton, P. A. (1997) *Biochemistry 36*, 4731−4738.
15. Colloc'h, N., Hajji, M. E., Bachet, B., L'Hermite, G., Schiltz, M., Prangé, T., Castro, B., and Mornon, J.-P. (1997) *Nat. Struct. Biol. 4*, 947−952.
16. Kahn, K., Serfozo, P., and Tipton, P. A. (1997) *J. Am. Chem. Soc. 119*, 5435−5442.
17. Bentley, R., and Neuberger, A. (1952) *Biochem. J. 52*, 694−699.

18. Ralston, G. (1993) *Introduction to Analytical Centrifugation*, Beckman Instruments, Inc., Fullerton, CA.
19. Alcock, N. W., Benton, D. J., and Moore, P. (1970) *Trans. Faraday Soc. 66*, 2210−2213.
20. Kuzmic, P. (1996) *Anal. Biochem. 237*, 260−273.
21. Peterman, B. F. (1979) *Anal. Biochem. 93*, 442−444.
22. Shrager, R. I. (1982) *Anal. Chem. 54*, 1147−1152.
23. Henry, E. R., and Hofrichter, J. (1992) *Methods Enzymol. 210*, 129−192.
24. Kankare, J. J. (1970) *Anal. Chem. 42*, 1322−1326.
25. Beechem, J. M. (1992) *Methods Enzymol. 210*, 37−54.
26. Straume, M., and Johnson, M. L. (1992) *Methods Enzymol. 210*, 87−105.
27. Mannervik, B. (1982) *Methods Enzymol. 87*, 370−390.
28. Lucas, K., Boland, M., and Schubert, K. R. (1983) *Arch. Biochem. Biophys. 226*, 190−197.
29. Suzuki, H., and Verma, D. P. S. (1991) *Plant Physiol. 95*, 384−389.
30. Bergmann, H., Preddie, E., and Verma, D. P. S. (1982) *EMBO J. 2*, 2333−2339.
31. Bielski, B. H., and Cabelli, D. E. (1995) in *Active Oxygen in Chemistry* (Foote, C., S., V. J., Greenberg, A., and Liebman, J. F., Eds.) pp 66−104, Blackie Academic & Professional, London.
32. Bongaerts, G. P. A., and Vogels, G. D. (1979) *Biochim. Biophys. Acta 567*, 295−308.
33. Davies, K. J. A., Sevanian, A., Muakkassah-Kelly, S. F., and Hochstein, P. (1986) *Biochem. J. 235*, 747−754.
34. Alamillo, J. M., Cárdenas, J., and Pineda, M. (1992) *J. Mol. Catal. 77*, 353−364.
35. Massey, V. (1994) *J. Biol. Chem. 269*, 22459−22462.
36. Maples, K. R., and Mason, R. P. (1988) *J. Biol. Chem. 263*, 1709−1712.
37. Yamamoto, K., Kojima, Y., Kikuchi, T., Shigyo, T., Sugihara, K., Takashio, M., and Emi, S. (1996) *J. Biochem. 119*, 80−84.
38. Zimmerle, C. T., and Frieden, C. (1989) *Biochem. J. 258*, 381−387.
39. Pfleiderer, W. (1974) *Liebigs Ann. Chem. 1974*, 2030−2045.
40. Bergmann, F., and Dikstein, S. (1955) *J. Am. Chem. Soc. 77*, 691−696.
41. Tokimitsu, Y., Ise, N., Tanaka, N., and Kunugi, S. (1995) *Bull. Chem. Soc. Jpn. 68*, 3277−3282.
42. Bruice, T. C. (1984) *Isr. J. Chem. 24*, 54−61.
43. Modric, N., Palkovic, A., Perina, I., and Poje, M. (1994) *Croat. Chem. Acta 67*, 347−360.
44. Palkovic, A., and Poje, M. (1990) *Tetrahedron Lett. 31*, 6101−6102.
45. Pfleiderer, W. (1957) *Chem. Ber. 90*, 2588−2603.
46. Bailey, S. W., and Ayling, J. E. (1983) *Biochemistry 22*, 1970−1978.
47. Benkovic, S. J., Sammons, D., Armarego, W. L. F., Waring, P., and Inners, R. (1985) *J. Am. Chem. Soc. 107*, 3706−3712.
48. Wrona, M. Z., Owens, J. L., and Dryhurst, G. (1979) *J. Electroanal. Chem. 105*, 295−315.
49. Lazarus, R. A., Dietrich, R. F., Wallick, D. E., and Benkovic, S. J. (1981) *Biochemistry 20*, 6834−6841.
50. Moad, G., Luthy, C. L., Benkovic, P. A., and Benkovic, S. J. (1979) *J. Am. Chem. Soc. 101*, 6068−6076.
51. Kemal, C., and Bruice, T. C. (1976) *Proc. Natl. Acad. Sci. U.S.A. 73*, 995−999.
52. Kemal, C., Chan, T. W., and Bruice, T. C. (1977) *J. Am. Chem. Soc. 99*, 7272−7286.
53. Maeda-Yorita, K., and Massey, V. (1993) *J. Biol. Chem. 268*, 4134−4144.
54. Hamilton, G. A. (1974) in *Molecular Mechanisms of Oxygen Activation* (Hayaishi, O., Ed.) pp 405−451, Academic Press, New York.
55. Jovanovic, S. V., and Simic, M. G. (1986) *J. Phys. Chem. 90*, 974−978.
56. Owens, J. L., Marsh, H. A., and Dryhurst, G. (1978) *J. Electroanal. Chem. 91*, 231−247.

BI980446G